*Egypt. J. Chem.* **Vol. 65**, No. 5 pp. 207 - 219 (2022)

**Egyptian Journal of Chemistry**

**http://ejchem.journals.ekb.eg/**

# Synthesis, Characterization of Lanthanum (III)/Terephthalate Metal-Organic Framework Copolymer, and Potential Use for Removal of Anionic and Cationic Exchange Contaminants

**Mohamed Saeed[1], Rabie Farag[2], Hesham Tantawy[3], Mustafa Mohsen[1]**

[1]*Egyptian armed forces, Cairo, Egypt*

[2]***Chemistry department, Faculty of Science, Al Azhar University, Cairo, Egypt***

[3]***Chemical Engineering Department, Military Technical College, Cairo, Egypt***

**Abstract**

Lanthanum (III)-terephthalic metal-organic framework copolymer (La-TPh CP) was synthesized by a solvothermal method and characterized by SEM/EDX, TEM, FTIR, Raman, BET, and XRD. Raman microscopyand XRD expose that terephthalic acid ($H_2$BDC) acts as a bidentate ligand towards lanthanum (La) (III) through the two carboxylate gropes. Both of FTIR and Raman microscopy emphasize the formation of coordination bonds between the electron-acceptor La (III) atoms and the electron-donor oxygen atoms. SEM shows that the (La-TPh CP) has a bar-like macro-structure with small dimensions, e.g., 200 nm. (La-TPh CP) structure is proposed to be cationic metal-organic framework and extremely water-stable. Due to these features, (La-TPh CP) was studded for the universal removal of cationic and anionic dyes, using synthetic cationic dye as methylene blue (MB) and an anionic dye as congo red (CR) in an aqueous solution. 5 mg/L MB and 40 mg/L CR was almost completely removed. Kinetic study for removal of CR shows the ideal order model is pseudo-second-order, and in the case of MB is pseudo-first-order.

*Keywords*: lanthanum(III)-terephthalic (La-TPh CP), metal-organic framework, ligand.

## 1- Introduction

The two-decade century witnessed the industrial raising, which effectively affects health improvements and the economy worldwide. This development put Earth's freshwater supply at risk. The contaminations were widespread in water with toxic chemicals such as organic dyes (anionic-cationic), for example (CR) as anionic dyes, and (MB) as cationic dyes. In developing nations, where environmental preservation enactment is minimal, the expansion acceleration of manufacturing has pervaded water sources, with pollutants endangering many people. Adsorption removal of contaminants from wastewater is a substantial application to target environmental conservation [1]. Dyes are among the most famous contaminants in wastewater of many industries such as textiles, paper, printing industries, chemicals, etc. [2]. Several catalysts are currently used for this aim, such as titanium dioxide[3], carbon tube[4], ferrites[5], and zeolite materials [6].

In the last twenty years, organic - inorganic crossbred materials (e.g., MOFs and CPs) have attracted awareness to this implementation because of controlling synthesis methods, purpose porosity, unique structural properties, and easy functionalization [1]. MOFs are a young branch of porous crystalline products with great possibilities in wastewater treatment [7].

MOFs are coordination networks of metal clusters linked using organic linkers. Incorporating inorganic and organic moieties allows regulation of the pores to mass ratios while ensuring the stability of the material in chemical structure [8]. These properties of MOFs allow them to have magnificent potential in many uses such as gas storage, biomedicine, and this research's work[9]. Lanthanum is one of the rare earth elements; a small amount from lanthanum added to steel makes its malleability efficient [10], superconductors, catalysts, and medical applications (e.g., MRI contrast agent)[11]. All chemicals which contain rare elements have comparable properties.

*Corresponding author e-mail: errmohammed123@gmail.com; (Mohamed Saeed).

Receive Date: 19 September 2021, Revise Date: 06 November 2021, Accept Date: 07 November 2021

DOI: 10.21608/ejchem.2021.96750.4537

In this field, terephthalate=1,4- benzene dicarboxylate (H2BDC) as an organic linker is very widespread due to its capability to create framework structures with eligible features. The presence of two carboxylic groups with an angle at 180° have a small barrier, and coupling with the aromatic ring allows it to become a stationary linker [12]. H2BDC can form different types of MOFs by coordination bonds with lanthanide metal centres.

The dyes presence as pollutants in the environment is wasted, but most of these components are also hazardous and very toxic[14,15]. Azo dyes are used in textiles, paper, cosmetics, and different industries [16], such as (MB) and (CR) [15], which can be dangerous not only for the environment but also for animals and humans[16].

CR is the first anionic synthetic dye with double azo (–N=N–) chromophores [17]. It is a very stable dye like other azo dyes because of its complex aromatic structure [18]. MB is a cationic synthetic dye; it is a heterocyclic aromatic compound[20,21], which has one azo (–N=) chromophores, and it is very stable because of its complex aromatic structure. MB cause acceleration of Heart rate, increased Heinz body formation, vomiting, shock, and necrosis of tissue in humans[21].

In this work, we have synthesized (La-TPh CP) by a solvothermal method and investigated their structural, application for universal removal of cationic and anionic pollutants from wastewater.

## Experimental

### *Materials, preparation, and characterizations*

The prime chemicals utilized for the preparation of the desired lanthanum-trephthalate metal-organic framework (La-TPh CP) were lanthanum (III), nitrate hexahydrate (99.99%, Sigma-Aldrich), and 1,4 dicarboxylic acid (98%, Sigma-Aldrich). N, N-dimethyl formamide (DMF) (99.8%, Sigma-Aldrich) was selected as solvent and reaction medium. Absolute ethanol (99.9%, Fisher Scientific) was used for the washing during all synthesis steps. Regarding preparation producers, a stoichiometric ratio was maintained between the reactants. Typically, 0.01mole of H2BDC and 0.01mole lanthanum nitrate hexahydrate were completely dissolved in 100ml of DMF after mixing for 30min with magnetic steering. The obtained solution was transferred to 200ml perfectly sealed Teflon tube and then subjected to hydrothermal heating in an oven at 120ºC for 18h. The obtained white crystals product was washed three times by DMF followed by three times by absolute ethanol. Finally, the washed product was dried at 80ºC for 24h[12].

The surface morphology of the synthesized La-TPh CP was investigated using SEM (EVO-MA10, ZEISS) and TEM (JEM-2100F, JEOL, Japan). Elemental composition was analyzed by energy dispersive X-ray (EDX) coupled with Scanning Electron Microscopy (SEM) device. Moreover, Raman spectroscopic measurements were performed on H2BDC and La-TPh CP using a dispersive Raman microscope (Bruker, Germany, model Senterra II). The objective (Nikon 20×) was used to focus the Raman excitation source (10 mW, 532nm neodymium-doped yttrium aluminium garnet (Nd: YAG) laser- Bruker, Germany).

Further, FTIR analysis of H2BDC and La-TPh CP was achieved via standard KBr pellet method on Perkin Elmer Spectrum One FTIR spectrometer, USA. The conformable spectra were tested between 500 cm–1and 3500 cm–1. Furthermore, the crystalline structure was inspected using XRD (XRD, D8 Advance, Bruker Corporation, Germany), using a copper tube (Cu Kα) and wavelength (λ) of 0.15419 nm at a speed of scanning 1 degrees/min and sample angle interval of 0.03 degree. The surface area of the samples was measured by using the BET (NOVA Station A) instrument. The specific surface area of the prepared samples was determined by the physical adsorption of Nitrogen gas on the solid surface and calculating the amount of adsorbate Nitrogen gas conformable to a monomolecular layer on the surface. The efficiency removal of dyes can be measured using a UV spectrophotometer (HACH double beam model DR-5000) at (λ) 496nm for CR and 664nm for MB[23].

### Adsorption experiment

The adsorption performance can be measured by using a Glas-col shaker (USA) under different conditions including; contact time (0–60)min, rate of shake (400)rpm, pH of dyes solution (4–10), adsorbent dosage La-TPh CP (30 – 60)mg/L, CR concentration (20–50)mg/L& MB (1-7)mg/L, ambient temperature (25°C) and a fixed volume of dyes solution (100)mL.

We transferred (100)mL of dye into a series conical flask containing the adsorbent dosage. We adjusted the initial pH values of dyes solutions by adding (0.1) M solution of HCl or NaOH. Separate 1 ml from the suspension adsorbent solution after every 10 minutes and centrifuge for 5 minutes, measure the absorbance using UV spectrophotometer at wavelength 496 nm for CR and 664nm for MB. Used the following equation to estimate the removal percentage (%) [19, 24].

$$\text{Removal} = \frac{C_\circ - Ct}{C_\circ} \times 100 \qquad (1)$$

where $C_\circ$ is the initial concentration of dyes (mg/L) and $C_t$ is the concentration of dye (mg/L) at time t (min) and final concentration.
The amount of the pollutant retained in the MOFs, $q_t$ (mg/g), can be calculated by the following equation [24]:

$$qt = C_\circ - Ct \quad \frac{V}{m} (2)$$

### 2.1 Adsorption kinetic models

Pseudo first and second-order kinetic models [25-27] were used to examine the controlling mechanism, determine reaction order and discuss the experimental data points of CR and MB adsorption from aqueous solutions.
The pseudo first order kinetic model is determined by the linear equation, as follows [27]:

$$dq/dt = K1\ (qe - qt) \qquad (3)$$

Where; pseudo-first-order constant ($min^{-1}$) is $k_1$, $q_e$, and $q_t$ (mg/g) are the values of the adsorbed capacity from dye at equilibrium and any time t (min), respectively.
By applying the conditions of $q_t = 0$ at $t = 0$ and $q_t = q_e$ at $t = t$, the integration of this equation can be lead to the following equation [49]:

$$\ln(qe - qt) = ln\ qe - K1t \qquad (4)$$

$k_1$ was calculated after plot relation between ln ($q_e - q_t$) and t; the value of k1 was determined from draw the slope and intercept.
The pseudo second order kinetic model is determined by the linear equation, as follows[24]:

$$\frac{t}{qt} = \frac{1}{K2q2e} + \frac{1}{qe}\ t \qquad (5)$$

where; $k_2$ is pseudo-second-order kinetic model constant (g/mg min).
Plot relation between $t/q_t$ and then calculate $q_e$ and $k_2$ from the draw intercept and the slope[28].

## 2- Results and discussion

### *2.1. Raman spectroscopy & FTIR Analysis*

Raman and FTIR analyses were performed to confirm the successful coordination of $H_2BDC$ with Lanthanum without any impurities incorporated in the obtained product. Raman spectra of $H_2BDC$and La-TPh CP are shown in figure (1-a), represents two main regions corresponding to lattice vibration and fingerprint. The first zone (below 200 $cm^{-1}$) is commonly representing the entire lattice vibrations. The presence of specific peaks in this zone should point out the crystalline nature of the specimen. According to the chart, $H_2BDC$ has two specific peaks in this zone at 67 and 105 $cm^{-1}$[29].

Meantime, La-TPh CP has three apparent peaks at 67, 94, and 121 $cm^{-1}$. The first two peaks are very close to $H_2BDC$ (67 and 94 $cm^{-1}$). These results emphasize the presence of the $H_2BDC$ molecule in the new La-TPh CP structure. The small shifts of La-TPh CP peaks to a higher energy band are associated with forming a new compound containing $H_2BDC$ring with another coordination bonds of higher energy.
The second zone of the Raman chart is referred to the fingerprint band, which covers the band from 200 to 1800 $cm^{-1}$. From this figure, $H_2BDC$ has strong peaks in this zone at 628, 829, 1125, 1174, 1279, 1431 and 1615 $cm^{-1}$ [29]. The weak peak at 628 $cm^{-1}$ should be designated to in-plane organic benzene ring bending [30], this peak has been disappeared and appeared two new weak peaks at 630 and 660 $cm^{-1}$, this emphasize the existence of the $H_2BDC$ rings in the new La-TPh CP and the shift toward the more energy band elucidate the rigidity occurred due to coordination. The obvious strong peak at 829 $cm^{-1}$ should be designated to an organic benzene ring and C-C bond stretching [30], this peak has been shifted to 856 $cm^{-1}$ toward the higher energy too and emphasize the resulted coordination. The weak peak appears at 1125 $cm^{-1}$ should be specified to in-plane C–H bending, or ring breathing [31], this peak is still found at the new La-TPh CP spectrum, which confirms the presence of the $H_2BDC$ rings in the new La-TPh CP. The weak peak at 1279 $cm^{-1}$ in the $H_2BDC$ spectrum should be nominated to the C-C inter-ring stretching [31]and disappeared in the La-TPh CP spectrum, which may be due to the stiffness from coordination. The short peak at 1431 $cm^{-1}$ and the large peak at 1615 $cm^{-1}$ should be designated to the symmetric stretching of the $COO^-$group [29] and still found in the new compound, corroborating the prior conclusion. In addition, it seems $H_2BDC$ incorporated in the La-TPh CP structure as $BDC^{-2}$. FTIR spectra of the prepared La-TPh CP and $H_2BDC$ were carried out within the frequency range of 500-4000 $cm^{-1}$as shown in figure (1-b).
The carboxylate group is discovered by vibrations of the two equivalent (C-O) bonds in in-phase or out-of-phase, leading to the asymmetric and symmetric stretch modes. The asymmetric stretch $\nu_{as}(COO^-)$ species is usually characterized by a wavenumber in the region 1600-1630 $cm^{-1}$[29], based on this work, we assign to $\nu_{as}(COO^-)$ band at 1630 $cm^{-1}$.These results confirming with Raman data that $H_2BDC$ incorporated in the La-TPh CP structure as $BDC^{2-}$.

Moreover, the bands at 1670 and 1571 $cm^{-1}$ are assigned to C=O stretching vibration originating from the carbonyl group of the $H_2BDC$ and C−C skeletal vibration of the aromatic ring [32, 33]. The sharp band at 1399 $cm^{-1}$ is assigned to the stretching vibration of (C−O). The bands appearing in the region 824 to 1124 $cm^{-1}$ can be referred to the stretching vibrations of asymmetric and symmetric (O−C=O) and the (C−O) stretching vibration of reacted form and unreacted $H_2BDC$ [32]. The peaks at 1154, 1106, and 1020 $cm^{-1}$

ascribed to the in-plane bending vibration of (C–H), while the peaks of out of plane bending vibration of (C–H) appear at 825, 723, and 668 $cm^{-1}$[33]. The significant bands at 1573 $cm^{-1}$, 1509 $cm^{-1}$, 1135 $cm^{-1}$, and 1111 $cm^{-1}$ are assigned to phenyl mode [29]. The presence shifting of the intense bands to (1548, 1500, 1106, 1020 $cm^{-1}$) in the La-TPh CP comparison with $H_2BDC$ indicates the formation of metal centres. The proposed coordinates of La (III) ions with the C=O group are lead to the peak of quadrant stretching of BDC benzene ring moved to the sharp, intensive peaks at 1630, 1608, 1548, 1440, 1154, 1106, 1020, 886, and 811 $cm^{-1}$. These results confirm that the connecting ligand is realized of terephthalic acid, which is deprotonated, and ($COO^-$) group reacts as an unidentate coordinate [34]. The significant change in this region of the Raman and FTIR spectra of the La-TPh CP confirms the variation of orientation of phthalate ions in the final product instead than pure terephthalic acid. Moreover, when a ligand coupled with a metal ion, new vibration modes not available in the unbound ligand may become IR or Raman active [35]. The previous analysis assigned to the confirmation of coupled of La (III) with $COO^-$ groups as expected merely because of the coordination of $COO^-$ of terephthalate molecules with La cations, which modification the electronic climate of the terephthalate.

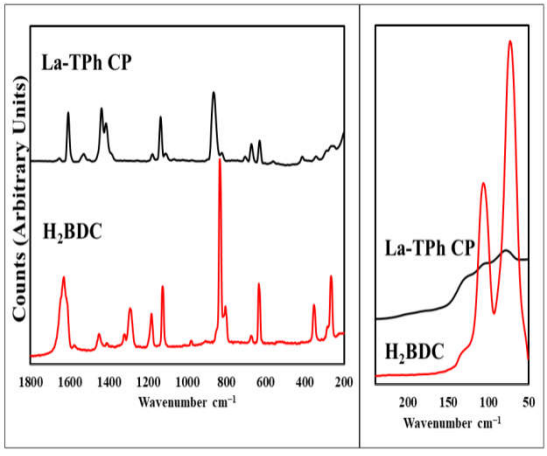


(a)

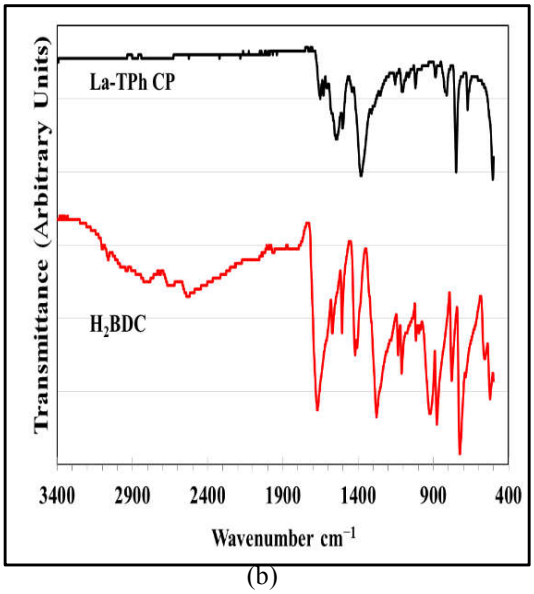


(b)

**Figure (1)** Raman spectra (a) and FTIR spectra (b) of La-TPh CP and $H_2BDC$

### *2.2. Morphological and EDX Analysis*

Morphological analysis of La-TPh CP via the SEM shown in Fig (2-a), The abstained nano-crystals have a rod shape with lateral less than 200nm and length in the order of few microns. The nano-crystals shape is almost identical and has edges. The EDAX analysis of the obtained products shows average relative percentages of main elements; C 64.85%, La 3.04%, O31.76%, and N 0.35 %. Moreover, the transmission electron micrograph of prepared La-TPh CP is showed in Fig (2-b and c). The results gained from TEM were comparable and well convention with those data obtained from SEM.

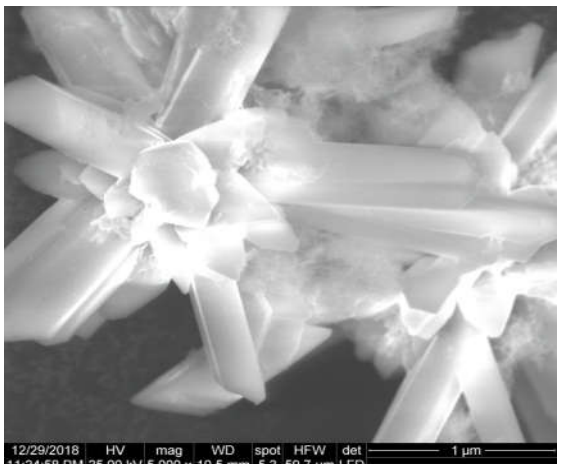


(a)

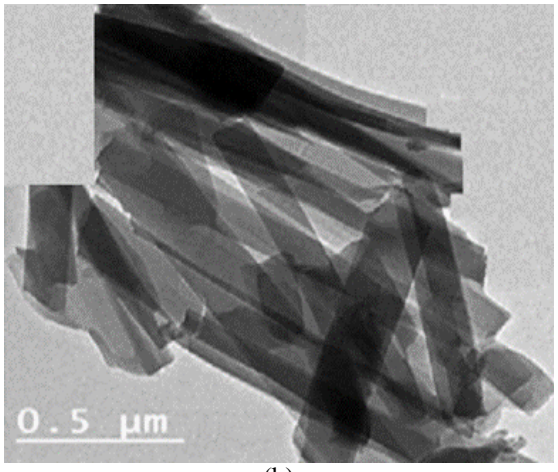


(b)

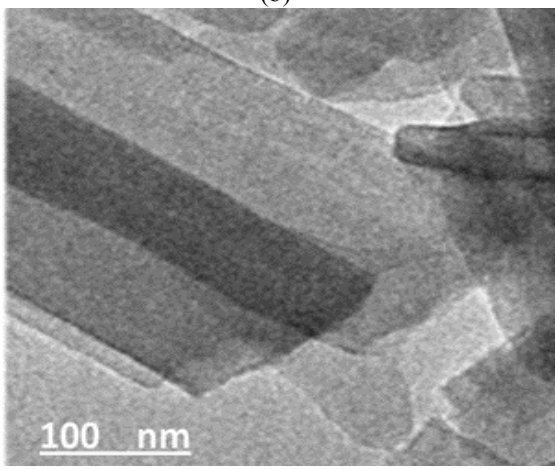


(c)

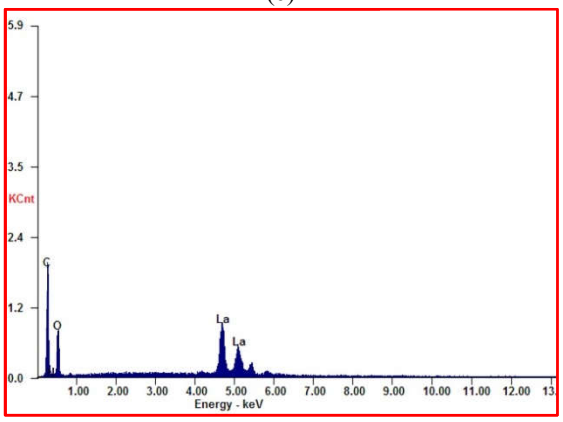


(d)

**Figure (2)** SEM; TEM and EDX image for La-TPh CP

### *2.2.1. XRD Analysis*

The observed X-ray Diffraction patterns of the product La-TPh CP are shown in figure (3). The X-ray diffraction patterns illustrate the triclinic phase of the La-TPh CP. The XRD pattern shows a clear peak around 2θ values ~ 9.22º, 9.54º,10.6º, 16.3º, 16.6º, 18.5º, 19º, 22.9º, 25.6º, 26º, 35.2º, 36.5º, 42º, 45º, and 50.5º[12, 36]. The most intense diffraction peak of La-TPh CP was observed at 2θ value 9.54º. The average crystallite size about 200 nm was determined from the diffraction peak broadening by Scherrer equation [37, 38], Dc= Kƛ/ßCosϴ, where K denotes the shape factor, which is usually around 0.9, ß denotes the diameter of the observed diffraction peak at its half maximum intensity, and ƛ is the wavelength of X-ray, where CuKα (ƛ =0.15406Å)[39]. Table (1) summarizes the obtained XRD data and represents the crystalline domain size in nm. According to supporting information, the estimated XRD pattern and the XRD pattern are in good agreement. [12].

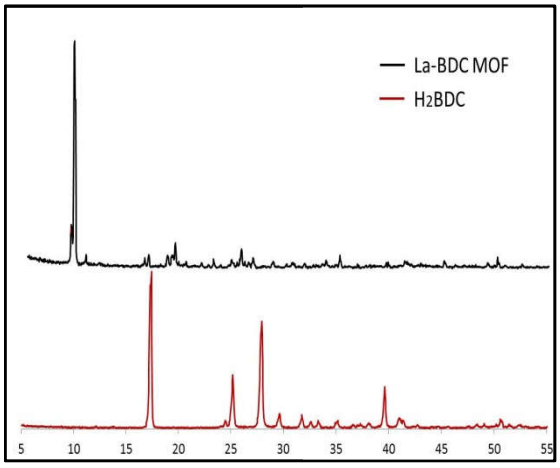


**Figure (3)** XRD patterns of the prepared La-TPh CP

**Table (1)** XRD data analysis summary of La-TPh CP

| *Sample* | *2θ* | *Domain size L(nm)* |
|---|---|---|
| La-TPh CP | **9.22** | |
| | **9.54** | **~ 200** |
| | **19** | |
| | **22.9** | |
| | **25.6** | |
| | **26** | |

### *2.2.2. La-TPh CP Surface area characterization*

The BET (Brunauer, Emmett and Teller) analysis of Nitrogen adsorption used to measured surface area of La-TPh CP, is 48.177 $m^2.g^{-1}$ which is significantly very small. This number should refer to the non-porosity of La-TPh CP and less efficiency during any applications of the adsorptive removal. However, the adsorption efficiency of La-TPh CP towards $CR^-$ (800 mg/g) concludes that La-TPh CP as adsorbent should be porous. Generally, most adsorbents have highly internal very small porous materials; the interior surface area of the adsorbent is higher than the outward surface area. Separation occurs because the polarity, variation in molecular mass, or shape causing the pores are very small to entry allowed the large molecules as $N_2$ or because

some molecules to be retained more strongly on the surface than another [40-42]. Also, the non-porous amorphous coordination polymer was reported as surface area (4.4 $m^2$ /g) as a high amplitude adsorbent of anionic dyes in an aqueous solution[43].

### *2.2.3. Adsorbents for Water Purification*

*2.2.3.1. Stability of CR and MB in water*

The reference point for this work was the stability profile of CR and MB in water to exam hydrolysis possibility. Figure 4 shows the hydrolysis profile of 40mg/L of CR and 5 mg/L of MB in water at 25ºC tested for 60min. As was expected and confirmed, CR and MB have reasonable stability in water with very low hydrolysis due to their high chemical stability [44, 45].

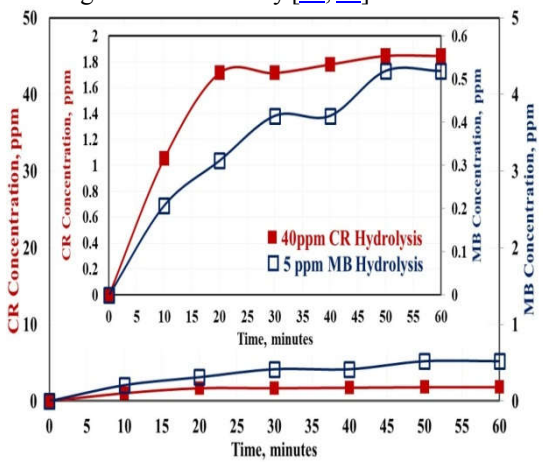


**Figure (4)** Stability of CR and MB in aqueous solution at pH6 for CR & pH 10 for M Blue and ambient temperature 25°C

### 3.5.1 Optimizing La-TPh CP MOF

To explore the optimum dose of the La-TPh CP achieving the maximum adsorption efficiency at a fixed initial concentration of CR and MB, different loading La-TPh CP was tested. Typically, 30, 40, 50, and 60 mg of La-TPh CP were selected at a fixed treatment time of 60 min and ambient temperature 25°C. Table 2 summarizes the net removal performance achievements concerning La-TPh CP loading.

Figure 5 shows the variation of removal efficiency of La-TPh CP with different loading concerning fixed CR initial concentration of 40mg/L and pH 6 at 25°C. It was obvious that increased loading of La-TPh CP from 30 to 60mg/L leading to increasing removal performance. It was clear that the initial concentrations fall very fast at the beginning within the first 10min leading to 93.3% removal for 60mg/L loading. Of course, lower loading leading a relatively lower initial drop leading to 65.8% removal for minimum loading 30mg/L. The maximum successful Removal reaches 97.1% for 60mg/L loading after 60 min. Furthermore, it was found that 50 and 60 mg/L loadings of La-TPh CP have a very comparable performance, which may be considered for economical processing.

Moreover, Figure 6 shows the variation of removal efficiency of La-TPh CP with different loading concerning fixed MB initial concentration of 5mg/L and pH 10 at 25°C. It was obvious that increased loading of La-TPh CP from 30 to 60mg/L leading to increasing removal performance. It was clear that the initial concentrations drop very fast within the first 10min leading to 55.6% removal for 60mg/L loading. Of course, lower loading leading a relatively lower initial drop leading to 27.5% removal for minimum loading 30mg/L. The maximum successful removal reaches 99.1% for 60mg/L loading after 60 min. Furthermore, it was found that 50 and 60 mg/L loadings of La-TPh CP have a very comparable performance, which may be considered for economical processing.

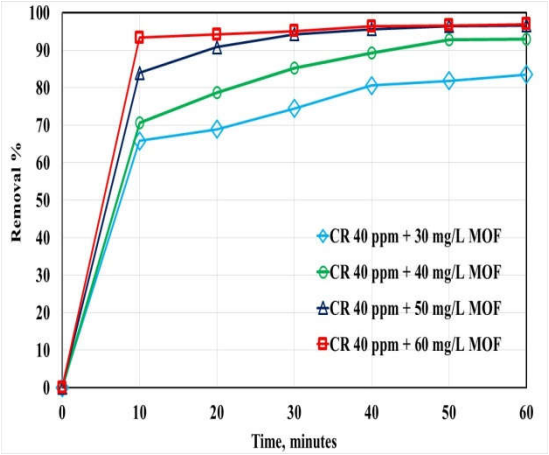


**Figure (5)** Adsorption profile of La-TPh CPMOF

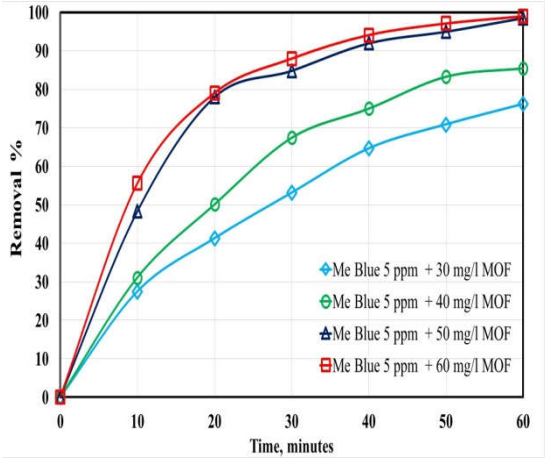


**Figure (6)** Adsorption profile of La-TPh CP

**Table (2)** Maximum adsorption efficiency of La-TPh CP at different loading 30, 40, 50, 60 mg/L with 40 mg/L CR and 5 mg/L MB

| | CR, 40 mg/L | | | | MB, 5 mg/L | | | |
|---|---|---|---|---|---|---|---|---|
| Dosing, mg/L | 30 | 40 | 50 | 60 | 30 | 40 | 50 | 60 |
| Efficiency, % | 83.5 | 92.9 | 96.6 | 97.1 | 76.1 | 85.5 | 98.6 | 99.1 |

### 3.5.2 Effect of the initial concentration of dyes

In this part of the work, the effect of the primary dye concentration on the adsorption process was conducted using various concentrations of CR and MB. Initial concentration was tested, varying 30 to 50 mg/L at pH 6 for CR dye and from 1 to 7 mg/L at pH 10 for MB dye. On the other hand, La-TPh CP loading was a fixed 50 mg/L, and experiments were performed at ambient temperature 25ºC. Table 3 summarizes the net removal performance achievements concerning initial dyes concentrations with fixed La-TPh CP loading.

Figure 7 shows the variation of removal efficiency of fixed loading of 50mg/L La-TPh CP with different initial concentrations of CR and pH 6 and 25°C. Increasing initial concentration of CR from 20 to50 mg/L leading to decreasing removal performance from 97.9 to 94.6%. Interestingly, the behaviour of 50mg/L La-TPh CP was remarkable overall; the 40 mg/L concentration has removal more than 95%. Similarly, Figure 8 represents the adsorption profiles for different concentrations of MB with the same fixed loading amount of La-TPh CP as in the case of CR. The concentration range under testing in the case of MB was taken from 1 to 7mg/L. As MB dye concentration increases from 1 to 5mg/L, the adsorption removal efficiency was stable at 98.9-98.6%. On the other hand, as MB dye concentration reaches 7mg/L, removal efficiency drops to 88.8%. This may be attributed to opacity increase and light scattering of catalyst particles to be effective at high concentration [46, 47].

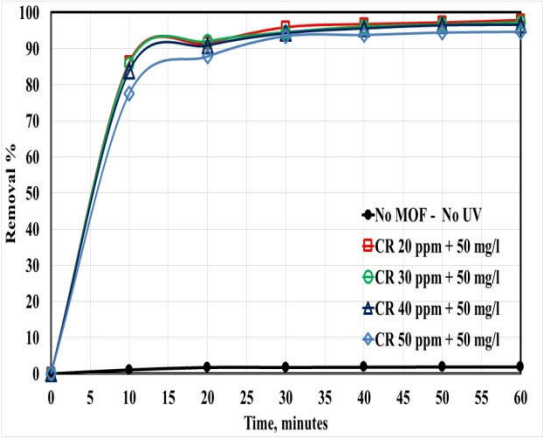


**Figure 7**Impact of initial concentration of CR on removal performance with 50mg/L La-TPh CP at pH 6 and ambient temperature 25ºC.

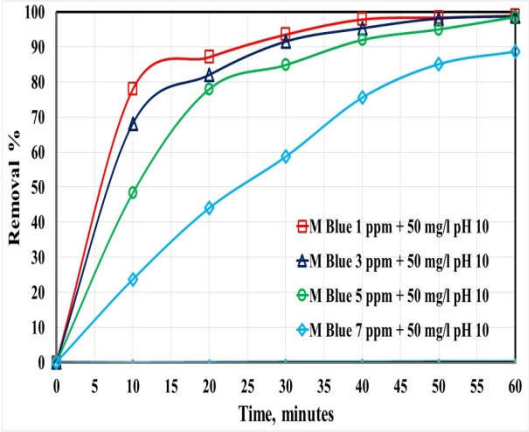


**Figure (8)**Impact of initial concentration of MB on removal performance with 50mg/L La-TPh CP at pH 10 and ambient temperature 25ºC.

**Table (3)** Maximum adsorption efficiency of La-TPh CP at a different initial concentration of MB and CR after 60 min at ambient Temp 25ºC

| | CR, pH6 | | | | MB, pH10 | | | |
|---|---|---|---|---|---|---|---|---|
| dye Concentration,mg/L | 20 | 30 | 40 | 50 | 1 | 3 | 5 | 7 |
| Adsorption efficiency, % | 97.9 | 97.3 | 96.6 | 94.6 | 98.9 | 98.6 | 98.6 | 88.8 |

*2.2.3.2. Effect of pH*

The impact of pH on removal performance via adsorption has an important significance in scaling up La-TPh CP utilization and elucidating any pH limitations for future applications. Since adsorption can be linked to the surface charge changes, hydrophobicity, net charge of pollutant, and changes in its adsorption modes, these may be affected significantly with the pH of the reaction medium. pH may lead to an amendment all of the rates. Furthermore, deviations in pH may present removal difficulties in the existence of long-living intermediates that toxic the adsorption is preferred[48].

In the present work, four values for pH were considered, covering the pH range from 4 to 12. The main aim of examining La-TPh CP's adsorption within the selected range is to confirm the possible application with the entire industrial waste pH range.

Figures (9 - 10) represent the effect of pH on adsorption deactivation profiles of 40 mg/L CR and 5 mg/L MB separately by 50 mg/L La-TPh CP at ambient temperature25°C. PH has a major impact on adsorption efficiency, which varied between 67.68% - 96.57% in case CR and varied between 28.63% - 98.55% in case MB over the examined pH range. In the case of CR, the adsorption efficiency is poor in more acidic and basic media but reaches neutral media. The efficiency at pH 4 is 81.19%, and pH 10 is 67.68% (poor adsorption), but at pH 6 is 96.57% and, pH 8 is 95.58% (reaches adsorption). The maximum removal of CR was achieved at pH 6, which could be attributed to a relative increase in $H^+$ ion level in the system concerning higher pH values[23]. Obviously, by absorbing $H^+$ ions at low pH, the surface of La-TPh CP acquire positive charge. Hereafter, the surface turns positively charged at low acidic medium, a meaningfully strong electrostatic interaction developed between the positively charged surface of La-TPh CP and CR molecule, which gives the highly adsorption of CR. As the pH of the medium rises, the negative charge spots rises and the positive charge spots declines. Due to the electrostatic repulsion, a negatively charged surface spot on the La-TPh CP does not prefer the adsorption an acidic dye molecule such as CR [49-51].

MB as a cationic dye, when dissolved in water gives positive charge ions. Thus, in an acidic medium, the MOF as sorbent gives a positively charged surface decreases the MB adsorbate's adsorption. When the pH of MB solution is raised, a negative charges on the surface are raised, leads to raised adsorption removal of MB due to raise to the electrostatic attraction between the positive charge of MB dye and the negative charge of La-TPh CP as adsorbent[53-54]. The adsorption efficiency of La-TPh CP at pH 4 is 28.63%, pH 6 is 29.46, and pH 8 is 48.96% (poor adsorption), but at pH 10 is 96.57% (reaches adsorption). The optimum removal of MB was achieved at pH 10.

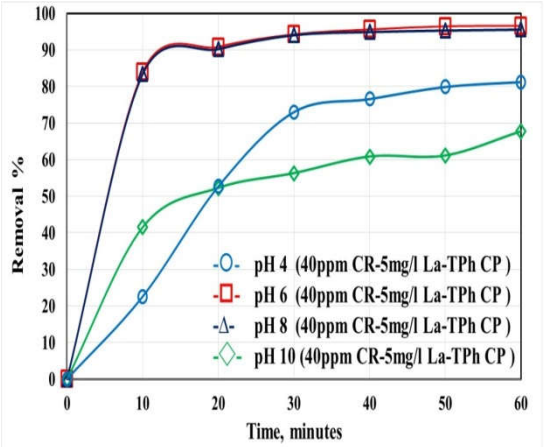


**Figure (9)** Effect of pH on removal profile of 40 mg/L CR by 50 mg/L La-TPh CP at 25°C

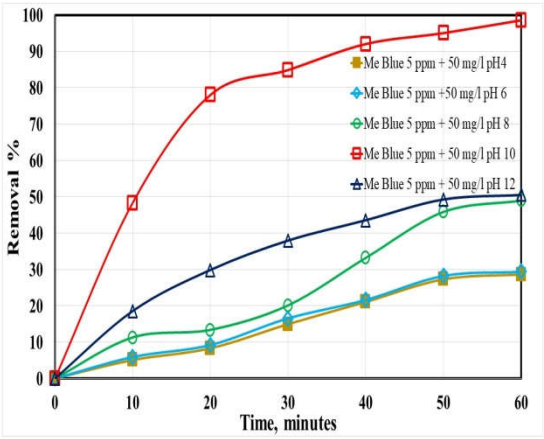


**Figure(10)**Effect of pH on removal profile of 5 mg/L MB using 50 mg/LLa-TPh CP at 25°C

*2.2.4. pH pzc of La-TPh CP and its Buffering Behaviour*

Figure (11) show the end of pH values of the solution for all initial pH values which used, were approached to specified pH, about pH 6.29. This same value was observed at equilibrium after 24 hrs of dipping the La-TPh CP in different pH solutions. The more practical pH value is measured during the catalysis process, that is, the first 2.5 hrs, and it was found to be about pH 6. In contrast, for blank solution (without La-TPh CP), the initial pH values were still constant until the end of the testes. The pH 6.29 can be considered as $pH_{pzc}$ for La-TPh CP and reflects its buffering behaviour. This property differs from traditional semiconductors, which keep acidity or basicity of the treated solutions and show positively

charged surface or negatively charged surface, respectively [56].

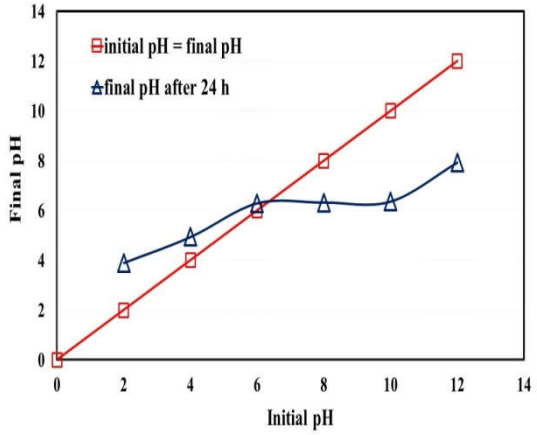


**Figure (11)** Determination of ($pH_{pzc}$) of La-TPh CP

The buffering behaviour of La-TPh CP would generate from its chemical structure. Therefore, it can be suggested that the La-TPh CP structure suffers from several defects where some BDC molecules are coordinated through the ortho-carboxylic group leaving other para-carboxylic groups coordination-free. Figure (12) displays the coordination environment of La(III) in defected sites of La-TPh CP and how it responds to acidic and basic aqueous media.

The −COOH moieties should be accountable for the buffering behavior. In neutral and acidic media (pH < 6.29), the −COOH group attractive to acidity, i.e., $H^+$, takes the shape of $-COOH^{2+}$ (−COOH / $-COOH^{2+}$ pair), leaving $OH^-$ that causes the raise in pH of the bulk solution to 6.29. On the other side, in the basic medium (pH > 6.29), the −COOH group responds to basicity, i.e., $OH^-$, giving $H_2O$ and forming −COO– (−COOH / −COO– pair). These attractive would be considered as a buffering reagent and have been explained in several studies, for example, He et al. developed and produced an organic linker that acts as a buffer guard to enhance water stability of the produced MOF (JUC-1000) by preserving its structural stability at different pH. They stated that the existence of the following pairs might cause the applied ligand to modify its total charge at different pH values (high – low): −O−/−OH, −OH/$-OH^{2+}$, −NH−/$-NH^{2+}$− and −NH/−N−[52-55].

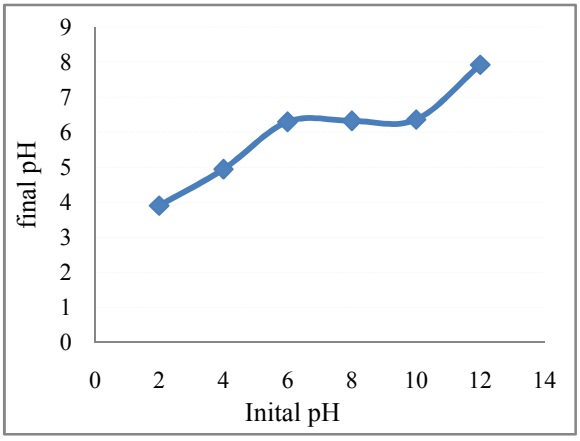


**Figure (12)** Description of buffering behaviour of La-TPh CP

### 2.2.5. Kinetic analysis:

This work applied the adsorption data of CR and MB on La-TPh CP to pseudo-first and second-order kinetic models. The correlation coefficient of the first-order kinetic model was (0.9665) for CR, (0.9844) for MB, and the second-order kinetic model was (0.9993) for CR, (0.9734) for MB. In the ceasing of CR, value of pseudo second-order kinetic correlation coefficient is larger than pseudo first-order kinetic, and This emphasized on The responsibility step for the interaction is chemisorption, equivalence forces occur through exchanging or sharing electrons [56, 57]. In the case of MB, the pseudo-first-order kinetic correlation coefficient is larger than pseudo-second-order kinetic.

Table (4) displays the obtained adsorption values for CR and MB at the surface of the La-TPh CP MOF. The results were lead to the ideal order model in the case of CR, where the correlation coefficient is very nearly to value 1 ($R^2$ = 0 .9993). In the case of MB, the results of first and second-order were close to each other, So that; the order of reaction can be first or second-order but first order nearest.

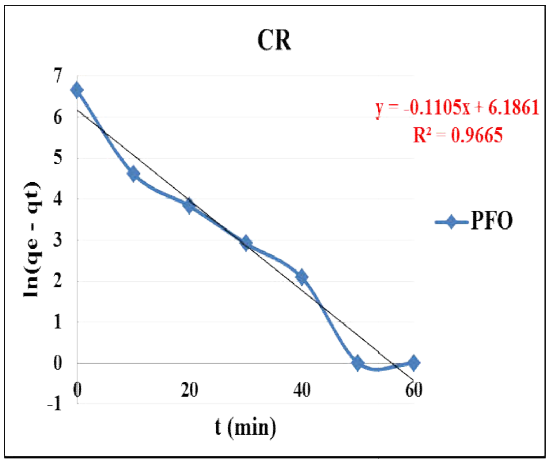


a) pseudo-First-order rate model

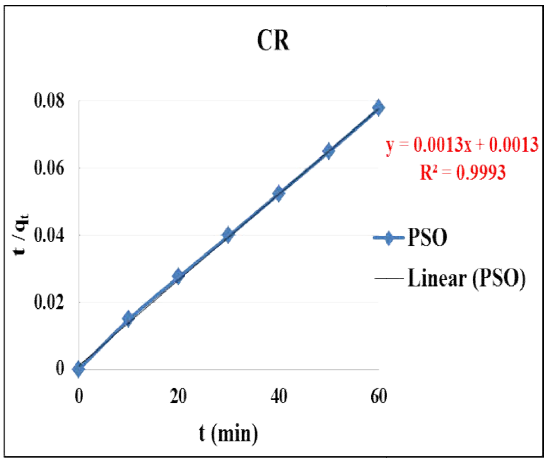


b) Pseudo-second-order rate model

**Figure (13)** Sorption kinetic Modelling of CR by La-TPh CP MOF

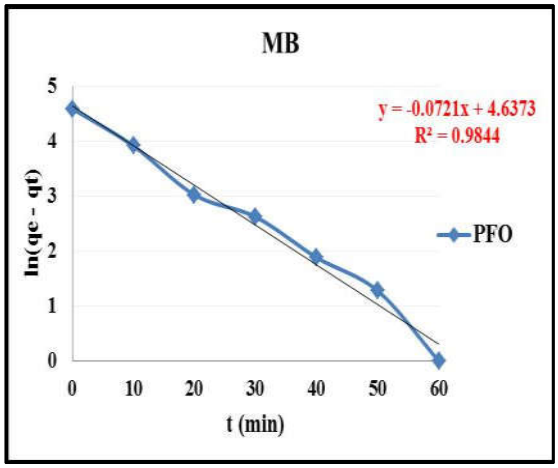


a) pseudo-First-order rate model

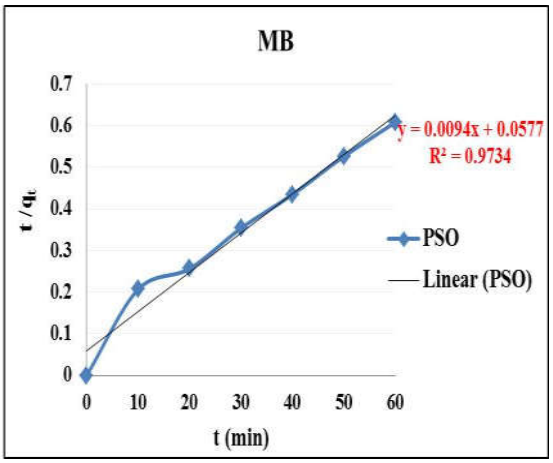


b) Pseudo-second-order rate model

**Figure (14)** Sorption kinetic Modelling of MB by La-TPh CP

**Table (4)** $R^2$ of pseudo-first and pseudo-second-order kinetics models for CR and MB

| pollutant | Pseudo-first order | | | Pseudo-second order | |
|---|---|---|---|---|---|
| | $R^2$ | $k_1$ | $q_e$ | $R^2$ | $k_2$ |
| CR, 40 mg/L | 0.9665 | 0.1105 | 772.6 | 0.9993 | 0.0013 |
| MB, 5 mg/L | 0.9844 | 0.072 | 98.6 | 0.9734 | 0.0017 |

## 3- Conclusion

In this study, the lanthanum metal organic framework (La-TPh CP) was successfully prepared from the precursor of a lanthanum nitrate hexahydrate salt and terephthalic acidusing solvothermal method. According to the results of characterization, it was concluded that the La-TPh CP structure. The test results of the adsorption activity to removal of CR and MB were (96.6% and 98.6 %) respectively, for 60 min. Kinetic study for removal of CR shows the ideal order model is pseudo-second-order, and in the case of MB is pseudo-first-order. Due to all that, La-TPh CP can use as a material for the universal removal of the cationic and anionic pollutants from wastewater.

## 4- References


1. Baraka, A., et al., A new cationic silver (I)/melamine coordination polymer,[Ag2 (melamine)] n2n+: Synthesis, characterization and potential use for aqueous contaminant anion exchange. Journal of Solid State Chemistry, 2019. **274**: p. 168-175.
2. Ramezanalizadeha, H. and F. Manteghia. Photocatalytic degradation of MB as an organic dye over a novel MOF/$BiFeO_3$ composite. in The 20th International Electronic Conference on Synthetic Organic Chemistry (ECSOC). 2016.
3. Fernandez-Ibanez, P., et al., Solar photocatalytic disinfection of water using titanium dioxide graphene composites. Chemical Engineering Journal, 2015. **261**: p. 36-44.
4. Das, R., et al., Carbon nanotube membranes for water purification: A bright future in water desalination. Desalination, 2014. **336**: p. 97-109.
5. Dhiwahar, A.T.; Maruthamuthu, S.; Marnadu, R.;. Sundararajan, M.; Manthrammel, M. A.; Shkir, M.; Sakthivel, P.; Reddy, V.R.M. Improved photocatalytic degradation of rhodamine B under visible light and magnetic properties using microwave combustion grown Ni doped copper ferrite spinel nanoparticles, Solid State Sciences, 2021, 113 : 106542
6. Margeta, K., et al., Natural zeolites in water treatment–how effective is their use. Water treatment, 2013. **5**: p. 81-112.
7. Raptopoulou, C.P., Metal-Organic Frameworks: Synthetic Methods and Potential Applications Materials 2021, 14: 310
8. Efome, J.E., et al., Insight studies on metal-organic framework nanofibrous membrane adsorption and activation for heavy metal ions removal from aqueous solution. ACS applied materials & interfaces, 2018. **10**(22): p. 18619-18629.
9. Dimitrova, D., Iron Based Metal Organic Frameworks as Photocatalysts for Chromium (VI) Degradation. 2015.
10. CHamsaz, M., G. Ronagi, and M.H. Arbab Zavar, Determination of Lanthanum in Human Blood Serum Using the Zero and First Derivative Spectrophotometr. Asian Journal of Chemistry, 2005.
11. Herrmann, H., et al., Aquatic ecotoxicity of lanthanum–a review and an attempt to derive water and sediment quality criteria. Ecotoxicology and Environmental Safety, 2016. **124**: p. 213-238.
12. Chen, W., et al., Synthesis and luminescence properties of brick-shaped lanthanum–organic frameworks with mesoporous and macroporous architectures. Luminescence, 2017. **32**(7): p. 1289-1293.
13. Li, S., et al., Water purification: adsorption over metal-organic frameworks. Chinese Journal of Chemistry, 2016. **34**(2): p. 175-185.
14. Chen, S., et al., equilibrium and kinetic studies of methyl orange and methyl violet adsorption on activated carbon derived from Phragmites australis. Desalination, 2010. **252**(1-3): p. 149-156.
15. Sulistiono, D., E. Santoso, and R. Ediati, Enhanced adsorption of methylene blue and Congo red from aqueous solutions by MCM-41/HKUST-1 composites. Asian J. Chem., 2019. **31**: p. 1675-1682.
16. Khanjani, S. and A. Morsali, Ultrasound-promoted coating of MOF-5 on silk fiber and study of adsorptive removal and recovery of hazardous anionic dye “congo red”. Ultrasonics sonochemistry, 2014. **21**(4): p. 1424-1429.
17. Diouri, K., A. Kherbeche, and A. Chaqroune, Kinetics of Congo red dye adsorption onto marble powder sorbents. Int J Innov Res Sci Eng Technol, 2015. **4**: p. 267-274.
18. Tapalad, T., et al., Degradation of Congo red dye by ozonation. Chiang Mai J Sci, 2008. **35**(1): p. 63-8.
19. Amar, I.A., et al., Adsorptive Removal of congo red dye from aqueous solutions using Mo-doped CoFe2O4 magnetic nanoparticles. Pigment & Resin Technology, 2021.
20. Umoren, S., U. Etim, and A. Israel, Adsorption of methylene blue from industrial effluent using poly (vinyl alcohol). J. Mater. Environ. Sci, 2013. **4**(1): p. 75-86.
21. Khodaie, M., et al., Removal of methylene blue from wastewater by adsorption onto ZnCl2 activated corn husk carbon equilibrium studies. Journal of Chemistry, 2013. **2013**.
22. Loera-Serna, S., et al., Elimination of Methylene Blue and Reactive Black 5 from Aqueous Solution Using HKUST-1. International Journal of Environmental Science and Development, 2017. **8**(4): p. 241.
23. Ponnusamy, S.K. and R. Subramaniam, Process optimization studies of Congo red dye adsorption onto cashew nut shell using response surface methodology. International Journal of Industrial Chemistry, 2013. **4**(1): p. 1-10.
24. Ahmed, D.N., et al., Waste foundry sand/MgFe-layered double hydroxides composite material for efficient Removal of Congo red dye from aqueous solution. Scientific reports, 2020. **10**(1): p. 1-12.
25. Lagergren, S.K., About the theory of so-called adsorption of soluble substances. Sven. Vetenskapsakad. Handingarl, 1898. **24**: p. 1-39.

26. Ho, Y.-S. and G. McKay, Pseudo-second order model for sorption processes. Process biochemistry, 1999. **34**(5): p. 451-465.
27. Luo, Y., et al., Synthesis of Cu-BTC Metal-Organic Framework by Ultrasonic Wave-Assisted Ball Milling with Enhanced Congo Red Removal Property. ChemistrySelect, 2018. **3**(41): p. 11435-11440.
28. Moeinpour, F., A. Alimoradi, and M. Kazemi, Efficient Removal of Eriochrome black-T from aqueous solution using NiFe 2 O 4 magnetic nanoparticles. Journal of environmental health science and engineering, 2014. **12**(1): p. 1-7.
29. Tan, K., et al., Stability and hydrolyzation of metal organic frameworks with paddle-wheel SBUs upon hydration. Chemistry of Materials, 2012. **24**(16): p. 3153-3167.
30. Hu, Y.H. and L. Zhang, Amorphization of metal-organic framework MOF-5 at unusually low applied pressure. Physical Review B, 2010. **81**(17): p. 174103.
31. Kumari, G., et al., Understanding guest and pressure-induced porosity through structural transition in flexible interpenetrated MOF by Raman spectroscopy. Journal of Raman Spectroscopy, 2016. **47**(2): p. 149-155.
32. Dikio, E.D. and A.M. Farah, Synthesis, characterization and comparative study of copper and zinc metal organic frameworks. Chem Sci Trans, 2013. **2**: p. 1386-1394.
33. Mohammadi, N. and F. Manteghi. Terephthalic acid as a linker in preparation of a new Ni-doped, Zn-based MOF. in The 19th International Electronic Conference on Synthetic Organic Chemistry. 2015. Multidisciplinary Digital Publishing Institute.
34. Gencheva, G., et al., Synthesis and structure of a new dimeric Pt (II)-Pt (III) complex with o-phthalic acid. Synthesis and reactivity in inorganic and metal-organic chemistry, 1998. **28**(4): p. 515-527.
35. Socrates, G., Infrared and Raman characteristic group frequencies: tables and charts. 2004: John Wiley & Sons.
36. Abdelbaky, M.S., et al., Synthesis, structures and luminescence properties of metal-organic frameworks based on lithium-lanthanide and terephthalate. Polymers, 2016. **8**(3): p. 86.
37. Shi, W., et al., Magnetic nano-sized cadmium ferrite as an efficient catalyst for the degradation of Congo red in the presence of microwave irradiation. RSC Advances, 2015. **5**(63): p. 51027-51034.
38. Ridha, S.M.A., X-ray studies and electrical properties of the zinc-substituted copper nanoferrite synthesized by sol-gel method. Int. J. Compos. Mater., 2015. **6**: p. 195-201.
39. Solomon, R., et al., Enhanced photocatalytic degradation of azo dyes using nano Fe 3 O 4. Journal of the Iranian Chemical Society, 2012. **9**(2): p. 101-109.
40. Adeyemo, A.A., I.O. Adeoye, and O.S. Bello, Metal organic frameworks as adsorbents for dye adsorption: overview, prospects and future challenges. Toxicological & Environmental Chemistry, 2012. **94**(10): p. 1846-1863.
41. Suzuki, M. and M. Suzuki, Adsorption engineering. Vol. 14. 1990: Kodansha Tokyo.
42. Allen, S. and B. Koumanova, Decolourisation of water/wastewater using adsorption. Journal of the University of Chemical Technology and Metallurgy, 2005. **40**(3): p. 175-192.
43. Li, B., et al., An amorphous coordination polymer with high adsorption ability for anionic dyes from aqueous solution. Science of Advanced Materials, 2013. **5**(4): p. 341-345.
44. Li, H., et al., Enhanced adsorptive Removal of anionic and cationic dyes from single or mixed dye solutions using MOF PCN-222. RSC advances, 2017. **7**(27): p. 16273-16281.
45. Jiang, C., et al., Efficient adsorptive Removal of Congo red from aqueous solution by synthesized zeolitic imidazolate framework-8. Chemical Speciation & Bioavailability, 2016. **28**(1-4): p. 199-208.
46. Beduk, F., M.E. Aydin, and S. Ozcan, Degradation of malathion and parathion by ozonation, photolytic ozonation, and heterogeneous catalytic ozonation processes. CLEAN–Soil, Air, Water, 2012. **40**(2): p. 179-187.
47. Carp, O., C.L. Huisman, and A. Reller, Photoinduced reactivity of titanium dioxide. Progress in solid state chemistry, 2004. **32**(1-2): p. 33-177.
48. Masoumi, S., G. Nabiyouni, and D. Ghanbari, Photo-degradation of azo dyes: photo catalyst and magnetic investigation of CuFe 2 O 4–TiO 2 nanoparticles and nanocomposites. Journal of Materials Science: Materials in Electronics, 2016. **27**(9): p. 9962-9975.
49. Mills, A. and S. Le Hunte, An overview of semiconductor photocatalysis. Journal of photochemistry and photobiology A: Chemistry, 1997. **108**(1): p. 1-35.
50. Pokropivny, V., et al., Introduction to nanomaterials and nanotechnology. 2007: Tartu University Press Ukraine.
51. Malik, P.K., Use of activated carbons prepared from sawdust and rice-husk for adsorption of

acid dyes: a case study of Acid Yellow 36. Dyes and pigments, 2003. **56**(3): p. 239-249.
52. Paul, A.K., G. Madras, and S. Natarajan, Adsorption–desorption and photocatalytic properties of inorganic–organic hybrid cadmium thiosulfate compounds. Physical Chemistry Chemical Physics, 2009. **11**(47): p. 11285-11296.
53. Meng, S., et al., Probing photonic effect on photocatalytic degradation of dyes based on 3D inverse opal ZnO photonic crystal. RSC Advances, 2013. **3**(38): p. 17021-17028.
54. Mahata, P., G. Madras, and S. Natarajan, Novel photocatalysts for the decomposition of organic dyes based on metal-organic framework compounds. The Journal of Physical Chemistry B, 2006. **110**(28): p. 13759-13768.
55. Mohsen, M., et al., A cadmium-imidazole coordination polymer as solid state buffering material: Synthesis, characterization and its use for photocatalytic degradation of ionic dyes. Journal of Solid State Chemistry, 2020. **289**: p. 121493.
56. Pathania, D., S. Sharma, and P. Singh, Removal of methylene blue by adsorption onto activated carbon developed from Ficus carica bast. Arabian Journal of Chemistry, 2017. **10**: p. S1445-S1451.
57. Tahir, M.H.M., S.E. Teo, and P.Y. Moh, Removal of methylene blue by iron terephthalate metal-organic framework/polyacrylonitrile membrane. Transactions on Science and Technology, 2017. **4**(1): p. 14-21.

**الملخص العربي:**

تم تحضير مركب شبكي متناسق معدني عضوي من عنصر اللانثانيوم مع حمض تيرفيثاليك ثم عمل توصيف للمركب الناتج بإستخدام جهاز التحليل بإستخدام حيود أشعة إكس وجهاز التحليل بإستخدام الأشعة تحت الحمراء وجهاز الميكروسكوب الالكتروني الماسح وجهاز التحليل بإستخدام حيود أشعة إكس لتأكيد التركيب الكيميائي للمركب المتكون ثم تحديد مساحة السطح بإستخدام جهاز تحديد مساحة السطح بإستخدام غاز النيتروجين.

تم إستخدام المركب الشبكي المتكون في معالجة مياه الصرف للتخلص من الأصباغ العضوية الانيونية والكاتيونية باستخدام صبغة الكونجو الأحمر بتركيز ٤٠ مجم/ لتر كمثال للأصباغ الانيونية ومركب أزرق الميثيلين بتركيز ٥ مجم/ لتر كمثال للأصباغ الكاتيونية مع دراسة العوامل المؤثرة علي عملية الامتصاص وكانت أعلي كفائة امتصاص لمركب الكونجو الاحمر 96.6 % ومركب أزرق الميثيلين 98.6%